Pressure-induced dehydration and reversible recrystallization of dihydrogen-bonded sodium borohydride dihydrate $NaBH_4 \cdot 2H_2O$

Satoshi Nakano,1, Hiroshi Fujihisa,2 Hiroshi Yamawaki,2 Yuki Shibazaki,3*

Takumi Kikegawa,3 Shin-ichi Orimo4,5

[1]National Institute for Materials Science (NIMS), Tsukuba, Ibaraki 305-0044, Japan

[2]National Metrology Institute of Japan (NMIJ), National Institute of Advanced Industrial Science and Technology (AIST), Tsukuba, Ibaraki 305-8565, Japan

[3]Photon Factory (PF), Institute of Materials Structure Science (IMSS), High Energy Accelerator Research Organization (KEK), Tsukuba, Ibaraki 305-0801, Japan

[4]Advanced Institute for Materials Research (WPI-AIMR), Tohoku University, Katahira 2-1-1, Aoba-ku, Sendai, 980-8577, Japan

[5]Institute for Materials Research (IMR), Tohoku University, Katahira 2-1-1, Aoba-ku, Sendai, 980-8577, Japan

ABSTRACT

Sodium borohydride dihydrate ($NaBH_4 \cdot 2H_2O$) forms through dihydrogen bonding between the hydridic hydrogen of the BH_4^- ion and the protonic hydrogen of the water molecule. High-pressure structural changes in $NaBH_4 \cdot 2H_2O$, observed up to 11 GPa through X-ray diffraction and Raman scattering spectroscopy, were analyzed to assess the influence of dihydrogen bonds on its crystal structure. At approximately 4.6 GPa, certain dihydrogen bonds were broken, leading to the decomposition of $NaBH_4 \cdot 2H_2O$ into ambient pressure phase of $NaBH_4$ (α-$NaBH_4$) and ice VII. Upon further compression beyond 6.6 GPa, $NaBH_4$ gradually transformed into its high-pressure phase, γ-$NaBH_4$. During decompression, γ-$NaBH_4$ reverted to α-$NaBH_4$ at the pressure between 4.4 and 2.7 GPa and subsequently reacted with ice VII, resulting in the recrystallization of $NaBH_4 \cdot 2H_2O$. This recrystallization, occurring during decompression from 4.4 GPa to 2.7 GPa, is identical to the starting sample and can be termed "decompression-induced recrystallization", highlighting the strength of the dihydrogen bonds in $NaBH_4 \cdot 2H_2O$. In addition, density functional theory calculations were used to evaluate the pressure dependence of hydrogen–hydrogen (H–H) distances in $NaBH_4 \cdot 2H_2O$. As pressure increased, the number of dihydrogen bonds within the unit cell rose from seven at near-ambient pressure to twelve at approximately 4.5 GPa just before the dehydration, indicating that each hydrogen atom in the water molecule formed dihydrogen bonds with around three hydrogens from the BH_4^- ions just prior to dehydration. Such pressure tuning of dihydrogen bonds may lead to the creation of new energy storage materials.

KEYWORDS: dihydrogen bond, sodium borohydride dihydrate, dehydration, sodium borohydride, ice VII, high-pressure, crystal structure

INTRODUCTION

In the pursuit of a carbon-free hydrogen energy society, extensive research has been conducted, leading to significant insights into the physicochemical properties and reactivity of hydrogen. Recent advances in materials research have highlighted the diversity of hydrogen valence, revealing that hydrogen can exhibit a wide range of valences, from positive to negative. This variation contributes to the diverse properties of hydrogen-containing materials.[1]

One key physicochemical phenomenon arising from this diversity is dihydrogen bonding. A dihydrogen bond forms when a protonic hydrogen with a positive valence ($H^{\delta+}$) and a hydridic hydrogen with a negative valence ($H^{\delta-}$) are attracted through electrostatic attractions.[2] The distance between the two hydrogen atoms in a dihydrogen bond is typically shorter than 2.4 Å, which is less than twice the van der Waals radius of hydrogen. While dihydrogen bonds have been widely studied in organic chemistry, their presence in inorganic materials remains relatively unexplored.

Ammonia borane (NH_3BH_3) is one of the few well-studied dihydrogen-bonded inorganic materials.[3] It is considered a potential hydrogen storage material, and its hydrogen absorption and desorption reactions have been extensively investigated. In NH_3BH_3, the hydrogen bonded to nitrogen is protonic, while the hydrogen bonded to boron is hydridic, resulting in molecules attraction and the formation of a molecular crystal under ambient conditions. By comparison, ethane (C_2H_6), which has a similar electronic structure, exists as a gas, underscoring the critical role of dihydrogen bonding in stabilizing NH_3BH_3 as a solid. Several studies have explored the relationship between dihydrogen bonding and the structural polymorphism of NH_3BH_3 under low temperature (LT), high-pressure (HP), and high-pressure/high-temperature (HP/HT) conditions.[4–11] At approximately 1.2 GPa and room temperature (RT), NH_3BH_3 undergoes a pressure-induced transformation to its first HP phase. Upon further compression, the number of dihydrogen bonds

increases from three to six at around 4 GPa while maintaining the same structure of the HP phase. The pressure dependence of the lattice parameters and volume of the HP phase changes before and after the pressure, which can be considered as an isostructural transition.[6,10,11] In addition, it has been observed that the HP/HT phases are almost the same density with or denser than the HP phases at the same pressure and RT, which is hypothesized to be the effects of dihydrogen bonding.[12]

Dihydrogen bonds should be studied across a broader range of inorganic materials and conditions. For instance, sodium borohydride dihydrate ($NaBH_4 \cdot 2H_2O$)[3] and lithium borohydride hydrate ($LiBH_4 \cdot H_2O$)[13] are both formed by dihydrogen bonds between the hydridic hydrogen of the BH_4^- ion and the protonic hydrogen of the H_2O molecule. In these complexes, the borohydride ion acts as a proton acceptor and the water molecule acts as a proton donor in the H–H bonds.[14] Complex hydrides, including borohydrides and alanates, contain anion clusters such as BH_4^- and AlH_4^-, with hydridic hydrogens influencing the surrounding space within the cluster. Consequently, it is expected that borohydrides and alanates will form dihydrogen bonds with molecules containing protonic hydrogen. Investigating these dihydrogen-bonded compounds and their structural transformations under wide HP or HP/HT conditions is crucial for advancing the understanding of dihydrogen bonding and for facilitating the synthesis of novel functional hydrides.

The synthesis of $NaBH_4 \cdot 2H_2O$ has been previously reported, indicating that it crystallizes at 0°C in $NaBH_4$–NaOH–H_2O and $NaBH_4$–$NaBF_4$–H_2O solutions and decomposes into $NaBH_4$ and an aqueous solution at 36.4°C.[15-19] Arkhangelskii et al. analyzed the thermal decomposition behavior of $NaBH_4 \cdot 2H_2O$ during heating up to approximately 500°C using thermogravimetric analysis, differential scanning calorimetry, and nuclear magnetic resonance.[20] In addition, it has been observed that $NaBH_4 \cdot 2H_2O$ forms when solid $NaBH_4$ powder captures H_2O vapor from a small

amount of water.[21, 22] Regarding the crystal structure, Custelcean and Jackson performed X-ray diffraction (XRD) measurements of $NaBH_4 \cdot 2H_2O$ and neutron diffraction measurements of $NaBD_4 \cdot 2D_2O$, identifying three types of dihydrogen bonds with O–H···H–B distances shorter than 2.4 Å.[23] Filinchuk and Hagemann synthesized single crystals of $NaBH_4 \cdot 2H_2O$, analyzing the crystal structures of the ambient phase at 100 K and 150 K, and also measured Raman and infrared (IR) spectra to identify vibrational modes.[24] Hamada et al. further calculated the charge density distribution using density functional theory (DFT), theoretically confirming the presence of dihydrogen bonds.[25]

Despite these studies, only the ambient phase of $NaBH_4 \cdot 2H_2O$ has been observed, with no transformation to a high-temperature (HT) or LT phase under ambient pressure (AP). As a result, the relationship between structural polymorphism and dihydrogen bonding remains unclear. Investigating the HP transformation of $NaBH_4 \cdot 2H_2O$ and the behavior of its dihydrogen bonds is therefore of significant interest. In this study, we examined the HP structural changes in $NaBH_4 \cdot 2H_2O$ using HP XRD and HP Raman scattering with diamond-anvil-cells (DACs). In addition, DFT calculations were conducted, using crystallographic parameters obtained from our experiments, to explore the influence of dihydrogen bonds on the observed structural changes.

EXPERIMENTAL SECTION

Preparation of sample and HP cell

DACs, equipped with a pair of 1/4-carat diamond anvils featuring 600-μm diameter cullets were used for XRD and Raman scattering measurements. An Inconel 600 foil, 300 μm thick, was compressed between the anvils to a thickness of 80–100 μm for use as a gasket. A 300-μm diameter

hole was drilled into the center of the gasket using an electrical discharge machine, forming the sample chamber in conjunction with the anvils.

A sample of $NaBH_4 \cdot 2H_2O$ (purity > 99.9%, Sigma-Aldrich, USA) was custom synthesized. All handling of the sample occurred in an argon atmosphere glove box at temperatures below 28°C to prevent decomposition. During grinding with a SiO_2 glass mortar, $NaBH_4 \cdot 2H_2O$ readily decomposed, producing $NaBH_4$. Therefore, a polycrystalline aggregate of the sample powder, approximately 250 μm in diameter (slightly smaller than the sample chamber), was selected and introduced into the sample chamber of the DAC without further crushing. To minimize external influences on the sample, no pressure medium was used. In addition, ruby balls with diameters of 15–20 μm were included in the sample chamber as pressure markers.

For comparison, HP XRD measurements were also performed on $NaBH_4$. Commercially available $NaBH_4$ powder (purity 99%, Sigma-Aldrich, USA) was loaded into the DAC's sample chamber. For this experiment, helium was introduced as a pressure medium using a gas-loading system.[26]

HP XRD measurements

Angle-dispersive XRD measurements were conducted using synchrotron radiation at the BL-18C and AR-NE1A beamlines of the Photon Factory at the High Energy Accelerator Research Organization (KEK-PF). The X-ray beam was monochromatized to 20 keV at BL-18C and 30 keV at AR-NE1A and introduced to the sample in the DAC through a collimator with a 100-μm diameter pinhole. Two-dimensional (2D) diffraction patterns were collected in transmission geometry using an image-plate detector at RT for pressures up to ~11 GPa with exposure times of approximately 15 minutes. The 2D diffraction patterns were integrated along the radial direction into a one-dimensional (1D) profile using the image analysis software, IPAnalyzer.[27] Lattice

parameters and unit cell volumes were calculated using PDIndexer.[27] The Rietveld analyses of the powder XRD patterns were performed using BIOVIA Materials Studio (MS) Reflex, version 2024 SP1.[28]

The sample pressure was estimated based on the shift of the fluorescence line of a ruby ball placed in the sample chamber. Fluorescence was excited using 532-nm laser light from a laser diode (LD)-pumped solid-state laser (Showa Optronics Co., Ltd., J050GS, 50 mW) and analyzed with a single monochromator (Princeton Instruments, Inc., Spectro Pro 2500i, f = 0.50 m) equipped with a 1200-grooves/mm grating. The emission was detected using a charge-coupled-device (CCD) detector (Acton, PIXIS100, active pixels: 1,340 × 100). The spectrograph was calibrated using neon and argon lamps, achieving a wavelength accuracy of ±0.02 nm.

After each compression or decompression cycle, the system was allowed to stabilize for ~10 minutes before the ruby fluorescence spectra were measured. These measurements were taken immediately before and after XRD measurements. The R1 line in the ruby fluorescence spectrum was fitted using a Gaussian function to determine the peak wavelength. The pressure was then calculated using the nonhydrostatic pressure equation by Mao et al.[29] for $NaBH_4 \cdot 2H_2O$ experiments without a pressure medium, and the hydrostatic pressure equation by Zha et al.[30] for $NaBH_4$ experiments with a helium medium. The average pressure before and after each XRD measurement was recorded as the final pressure value for the corresponding experiment.

HP Raman scattering measurements

A continuous-wave fiber laser with a wavelength of 488 nm (Azur Light Systems, ALS-BL-488-1-I-SF, 1W) was used as the excitation source for the Raman scattering experiments, with 20 mW of power delivered to the sample surface. The incident laser beam was focused to a diameter of approximately 10 μm on the sample through the diamond anvil window using a 45× objective

lens. Raman scattering spectra were collected using a single monochromator spectrometer (Jobin-Yvon/Atago-Bussan T64000) equipped with a 600-grooves/mm diffraction grating, offering a wavenumber resolution of 2 cm^{-1}/pixel. The spectra were recorded for durations of 40–100 s using a silicon-based CCD detector (Spectrum ONE, ISA Inc.) with 2000 × 800 pixels, cooled electrically to 140 K. The wavenumber scale was calibrated using a neon lamp.

The same apparatus used for Raman scattering measurements was also employed for pressure determination. The procedure for measuring ruby fluorescence and calculating pressure followed the same methodology as described for the XRD measurements.

Computational details of the structural analysis

In the powder XRD experiment and Rietveld analysis, the diffraction intensity is weak due to the low atomic numbers of sodium, boron, and oxygen. Furthermore, information such as the coordinates of hydrogen atoms, the orientation of BH_4^- and H_2O, and the hydrogen–hydrogen (H–H) bond distances could not be obtained. To overcome these limitations, MS-CASTEP[31] was used to perform full atomic structure optimization while fixing the lattice constants to the results obtained from the Rietveld analysis.

The Perdew-Burke-Ernzerhof (PBE) exchange-correlation functionals within the generalized gradient approximation framework[32] and on-the-fly generated norm-conserving pseudopotentials[33] were utilized. A plane-wave basis set with a cut-off energy of 1020.0 eV was employed. A 4 × 2 × 2 Monkhorst-Pack grid[34] was selected for the k-point sampling, resulting in k-separations of approximately 0.04 $Å^{-1}$. The convergence criteria included a maximum force tolerance of 0.003 eV/Å, a maximum atomic displacement of 3.0×10^{-4} Å, and an energy convergence tolerance of 3.0×10^{-6} eV/atom.

Basically, the intermolecular force in this system is the Coulomb force, and the Tkatchenko-Scheffler scheme[35] was added as dispersion corrections to improve the accuracy of the interatomic distances. The valence electrons used in the DFT calculations were as follows: for Na, $2s^2\ 2p^6\ 3s^1$; for B, $2s^2\ 2p^1$; for H, $1s^1$; and for O, $2s^2\ 2p^4$. The $1s^2$ electrons of Na, B, and O were treated as core electrons and represented using pseudopotentials.

RESULTS AND DISCUSSION

HP XRD measurements during the compression process

The pressure dependence of the XRD pattern of $NaBH_4 \cdot 2H_2O$ is presented in Figure 1. Initially, the diffraction pattern corresponded primarily to the diffraction lines of $NaBH_4 \cdot 2H_2O$, consistent with previous reports.[24] However, because of the absence of a pressure medium, the peak intensity ratios deviated from simulated data, likely due to preferred orientation effects.

As pressure increased up to 4.0 GPa, the XRD peaks of $NaBH_4 \cdot 2H_2O$ shifted to higher angles. At 4.6 GPa, the diffraction pattern changed significantly and new peaks emerged. By 5.1 GPa, the original $NaBH_4 \cdot 2H_2O$ peaks had nearly disappeared, and the newly emerged peaks could be assigned to the AP phase of $NaBH_4$ (α-$NaBH_4$: *Fm*-3*m*)[36] and ice VII.[37] This indicates that $NaBH_4 \cdot 2H_2O$ underwent pressure-induced dehydration, producing $NaBH_4$ and H_2O, as described by the following equation (1).

$$NaBH_4 \cdot 2H_2O \rightarrow NaBH_4 + 2H_2O \quad (1)$$

This pressure-induced dehydration is accompanied by the cleavage of the dihydrogen bond between the BH_4^- cluster and the H_2O molecule. It is plausible that H_2O precipitated as ice VII, which is the thermodynamically stable phase under these dehydration conditions, according to the pressure-temperature (P-T) phase diagram of H_2O.[38] In this pressure-induced dehydration, the

hydrogens of the water molecules broke the dihydrogen bonds with the hydrogens of the BH_4^- ions and formed hydrogen bonds with the oxygens of adjacent water molecules, crystallizing into ice VII.

To better understand the pressure-induced dehydration of $NaBH_4 \cdot 2H_2O$, it is important to estimate the crystallite sizes of the decomposition products. While the Scherrer method[39] is commonly used for determining crystallite size from XRD patterns, we applied the Williamson-Hall method[40] to separate the strain component from peak broadening, as strain effects could not be ignored in the current experiments.

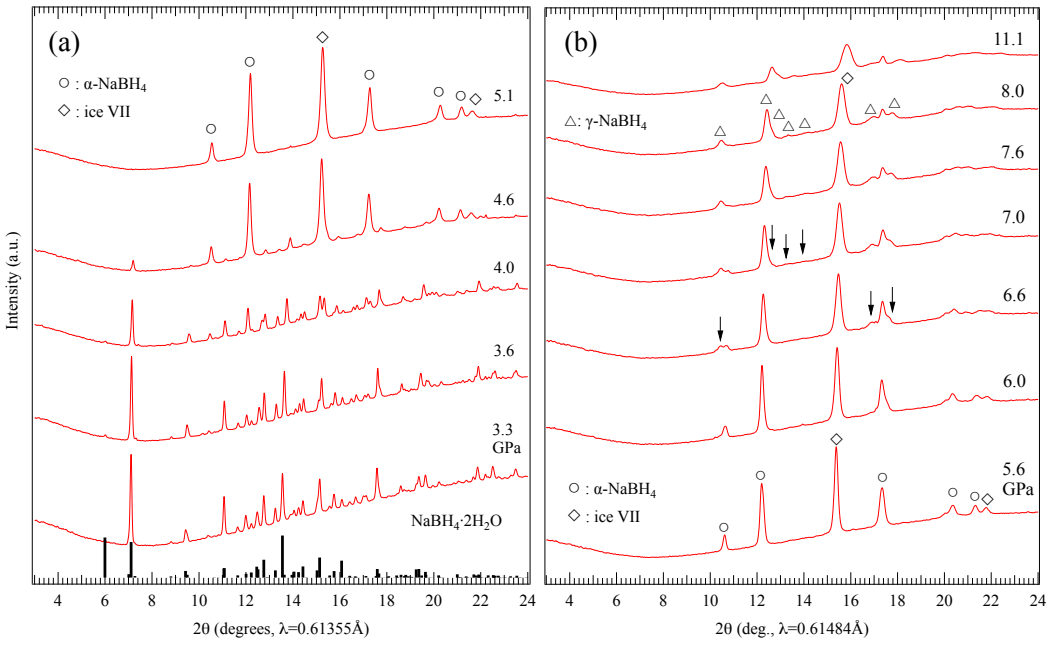

Figure 1. Pressure dependence of the XRD pattern of $NaBH_4 \cdot 2H_2O$ up to (a) 5.1 GPa and (b) 11.1 GPa during compression. Circle, square, and triangle symbols represent α-$NaBH_4$, ice VII, and γ-$NaBH_4$, respectively. Black bars in (a) show the positions and intensities of the simulated Bragg peaks of $NaBH_4 \cdot 2H_2O$ at 3.3 GPa. Black arrows in (b) indicate the appearance of new peaks.

The five peaks of α-$NaBH_4$ and the two peaks of ice VII observed at 5.1 GPa, where the dehydration of $NaBH_4 \cdot 2H_2O$ was completed, were fitted with Lorentz functions to determine peak positions and full width at half maximums (FWHMs). A Williamson-Hall plot was generated, as shown in Figure S1. From this analysis, the average crystallite size (d) of α-$NaBH_4$ was estimated to be 39 nm, with a lattice distortion component (Cε) of 0.011, while d of ice VII was determined to be 24 nm, with Cε = 0.009. Since this estimation does not account for instrumental contributions, the actual average crystallite sizes are likely larger. For comparison, d and Cε of commercial α-$NaBH_4$ powder at AP were calculated to be d = 52 nm and Cε = 0.0007, respectively. These results, as shown in Table S1, suggest that $NaBH_4$ crystallites decomposed from $NaBH_4 \cdot 2H_2O$ are smaller than those of commercial α-$NaBH_4$, and the crystallites of ice VII are even smaller.

Pressure-induced transformation of $NaBH_4$ decomposed from $NaBH_4 \cdot 2H_2O$

Upon further compression to 11 GPa, the ice VII phase persisted, but the FWHM of its peaks increased, as shown in Figure 1(b). In contrast, $NaBH_4$ exhibited a pressure-induced transformation between 6.6 GPa and 8.0 GPa. This change in the XRD pattern is similar to that reported by Filinchuk et al.[41] In other words, $NaBH_4$ decomposed from $NaBH_4 \cdot 2H_2O$ undergoes the same structural transformation as pure $NaBH_4$, regardless of the presence of H_2O during further compression.

Kumar et al.[42] reported that $NaBH_4$ undergoes a pressure-induced transformation from α-$NaBH_4$ to a HP phase (β-$NaBH_4$: $P42_1c$) at 6.3 GPa, followed by a second HP phase (γ-$NaBH_4$: *Pnma*) at 8.9 GPa. However, Filinchuk et al.[41] did not clearly observe these two transformations, likely due to the nonhydrostatic pressure conditions caused by the absence of a pressure medium. Kumar et al. used silicone fluid as a pressure medium, which does not react with $NaBH_4$, but it loses its hydrostatic properties above 3 GPa.[43] Marizy et al.[44] performed HP experiments on $NaBH_4$ using

neon (with a solidification pressure of 4.8 GPa) as a pressure medium, but they did not clearly describe the phase transition pressure from β-$NaBH_4$ to γ-$NaBH_4$. In this study, we observed the pressure-induced transformation of $NaBH_4$ using helium as a pressure medium up to ~8 GPa via XRD. Helium, with a solidification pressure of 11.5 GPa,[45] ensured that the experiments were conducted under completely hydrostatic conditions. As shown in Figure S2, we found that the transformation from α-$NaBH_4$ to β-$NaBH_4$ began at 5.5 GPa and completed at 6.4 GPa, with the subsequent transformation to γ-$NaBH_4$ starting at 7.7 GPa.

In the case of $NaBH_4$ formed by the dehydration of $NaBH_4 \cdot 2H_2O$, the β-$NaBH_4$ phase was not clearly observed, consistent with the findings of Filinchuk et al. This suggests that under low-hydrostatic conditions, in the absence of a pressure medium, the transition from α-$NaBH_4$ to γ-$NaBH_4$ may occur gradually, bypassing the β-$NaBH_4$ phase.

HP XRD measurements during decompression

Figure 2 illustrates the changes in the XRD pattern during the decompression process from 11 GPa to nearly AP. γ-$NaBH_4$ reverted to α-$NaBH_4$, which subsequently recrystallized into $NaBH_4 \cdot 2H_2O$, identical to the starting sample, during decompression from 4.4 GPa to 2.7 GPa. This recrystallization follows the reaction shown in the following equation (2), a process we refer to as "decompression-induced recrystallization."

$$NaBH_4 + 2H_2O \rightarrow NaBH_4 \cdot 2H_2O \quad (2)$$

This recrystallization suggests that it is thermodynamically more stable for $NaBH_4$ and H_2O to form dihydrogen bonds and crystallize as $NaBH_4 \cdot 2H_2O$ rather than remain as separate entities. The strength of the dihydrogen bond likely plays a crucial role in this stability.

It is noteworthy that the recrystallization of $NaBH_4 \cdot 2H_2O$ occurred without the presence of a fluid. As discussed in the introduction, at AP, $NaBH_4 \cdot 2H_2O$ typically forms through isothermal

reactions in either a liquid solution or the vapor phase.[15–19, 21] However, in this experiment, "decompression-induced recrystallization" occurred at pressures of 2.7 GPa or higher, where H_2O exists as solid ice VII.

In this recrystallization process, even though it occurs as a solid-state reaction, water molecules appear to move freely between Na^+ and BH_4^- ions in $NaBH_4$. This may indicate that the electrostatic interaction between the protonic and hydridic hydrogens extends beyond the molecular scale, enabling the crystallization of $NaBH_4 \cdot 2H_2O$.

Arkhangelskii et al.[21] noted slight differences between the XRD patterns of $NaBH_4 \cdot 2H_2O$ synthesized from the liquid phase and those formed through reactions with vapor-phase H_2O. However, in this study, no significant differences were observed between the diffraction patterns

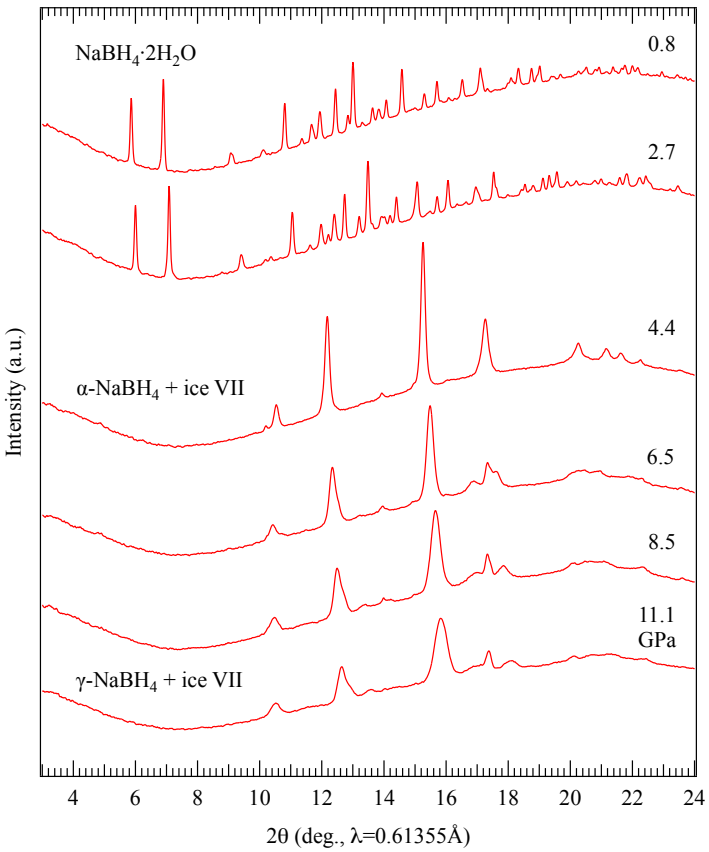

Figure 2. Pressure dependence of the XRD pattern during decompression from 11.1 GPa.

of $NaBH_4 \cdot 2H_2O$ obtained through “decompression-induced recrystallization” and those synthesized from an aqueous solution.

HP Raman scattering measurement

The results of the HP Raman scattering measurements are presented in Figure 3. The H_2O libration mode, H–O–H bending mode, and O–H stretching mode weakened above 4.1 GPa, and nearly disappeared by 4.9 GPa. In addition, the number of peaks in the B–H stretching mode decreased above 4.1 GPa, indicating that the number of distinct B–H stretching modes of BH_4^- ions diminished as H_2O was released. These observations align with the XRD results, which showed the dehydration of $NaBH_4 \cdot 2H_2O$ occurring between 4.0 and 4.6 GPa. As compression continued, the shape of the B–H stretching modes gradually changed between 6.3 and 8.2 GPa, corresponding to the XRD results that indicated a gradual phase transformation from α-$NaBH_4$ to γ-$NaBH_4$ between 6.6 GPa and 8.0 GPa.

During decompression, the spectral changes were reversible, though with a slight hysteresis, which also corresponds to the XRD findings.

A schematic diagram illustrating the phase changes derived from the HP XRD and Raman scattering results is shown in Figure 4.

It is valuable to compare the pressure-induced dehydration reactions of dihydrogen-bonded $NaBH_4 \cdot 2H_2O$ with those of hydrogen-bonded hydrous compounds. A comparison of the pressure-induced dehydration at RT of hydrogen-bonded hydrous compounds reported previously with the present results is discussed in the Supporting Information.

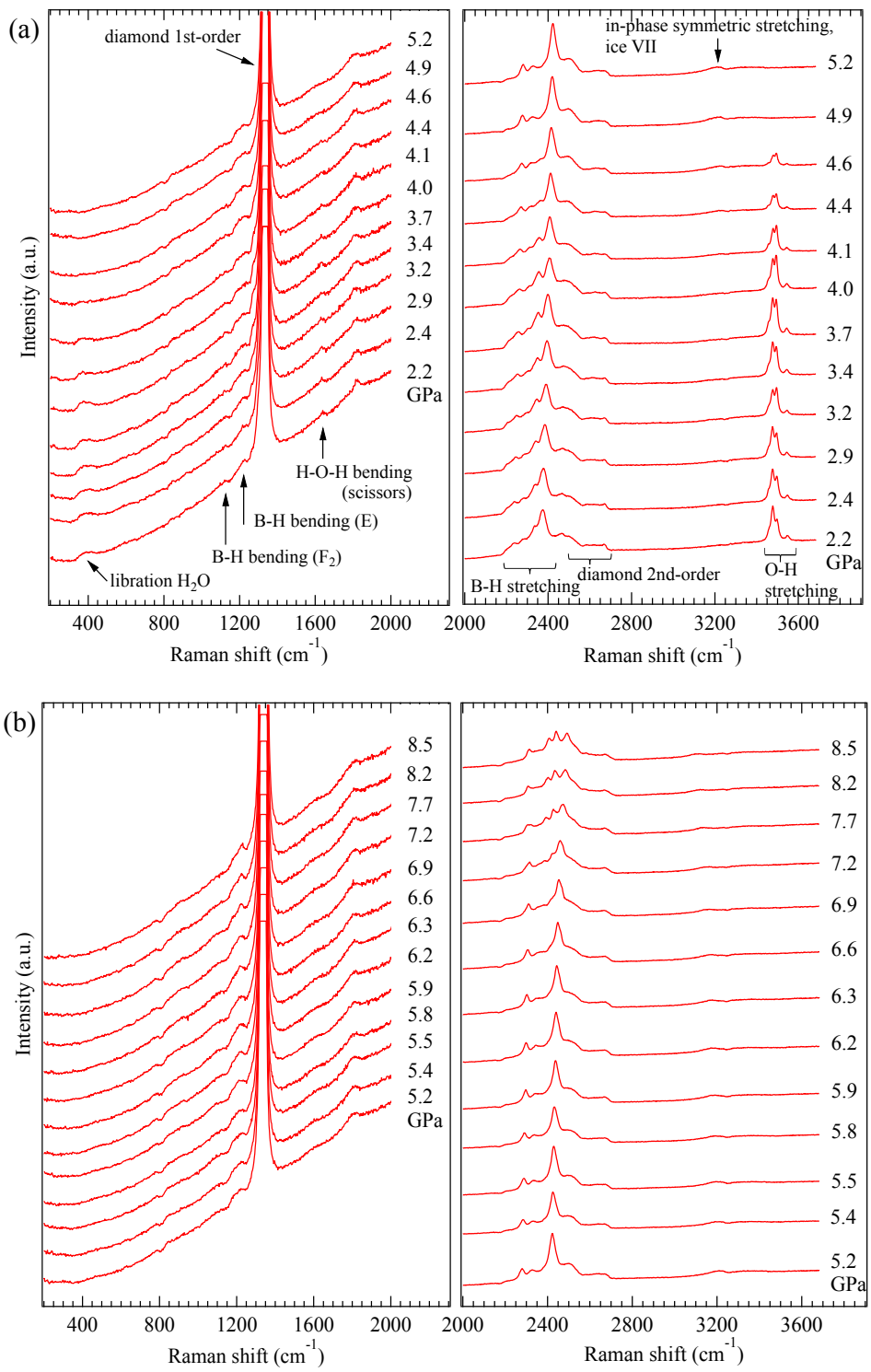

Figure 3. Pressure dependence of the Raman scattering spectrum of $NaBH_4 \cdot 2H_2O$ up to (a) 5.2 GPa and (b) 8.5 GPa during compression. The Raman modes were identified with reference to the previous report by Filinchuk, et al.[24]

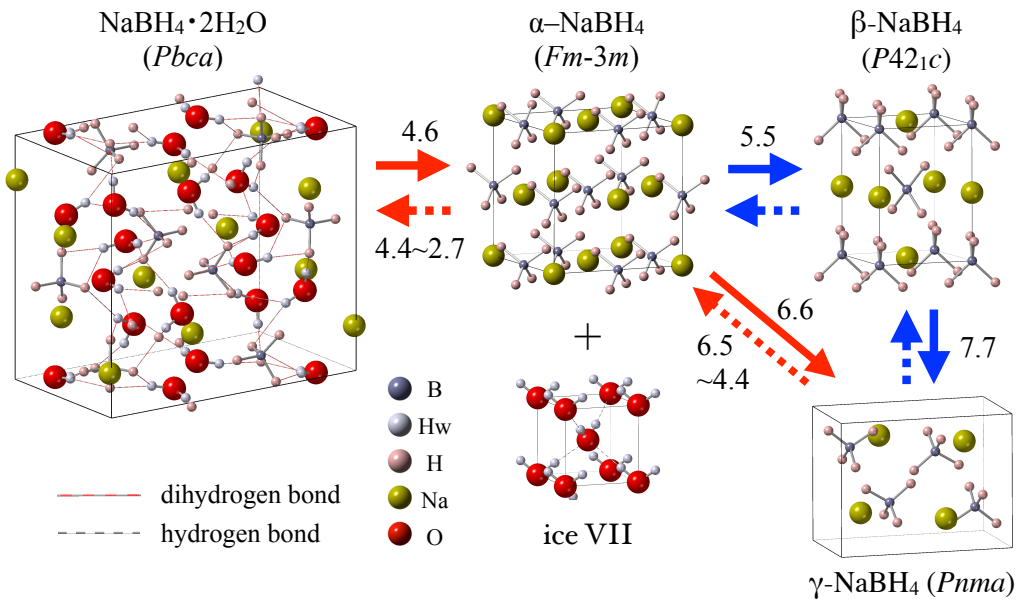

Figure 4. Schematic of the phase changes in $NaBH_4 \cdot 2H_2O$ and $NaBH_4$, based on HP XRD and Raman scattering results. Solid arrows represent structural changes during compression, and dashed arrows represent changes during decompression. Pressure values are given in GPa. $NaBH_4 \cdot 2H_2O$ decomposed into α-$NaBH_4$ and ice VII under pressure, and α-$NaBH_4$ transformed into γ-$NaBH_4$ (red arrow). In helium medium, α-$NaBH_4$ transformed into β-$NaBH_4$ and then γ-$NaBH_4$ (blue arrow). These changes were reversible with hysteresis.

Pressure dependence of the volumes

The pressure dependence of the volume per formula unit (f. u.), calculated from the lattice parameters of the sample, is shown in Figure 5. V($NaBH_4 \cdot 2H_2O$) represents the volume of 1 f. u. of $NaBH_4 \cdot 2H_2O$ before dehydration, while V("$NaBH_4 \cdot 2H_2O$") corresponds to the combined volumes of 1 f. u. of $NaBH_4$ and two f. u. of ice VII observed after the dehydration of $NaBH_4 \cdot 2H_2O$. For comparison, the sum of the volumes of $NaBH_4$ and H_2O measured separately is also shown; V($NaBH_4$ + $2H_2O$) corresponds to the sum of the volumes of 1 f. u. of $NaBH_4$ and 2 f. u. of H_2O

(represented by the black dashed line). The volume of $NaBH_4$ alone was calculated from our current XRD results (Figure S2), while the volume of H_2O alone was obtained from literature data.[46,47] In addition, the pressure dependences of the volumes of $NaBH_4$ and H_2O decomposed from $NaBH_4 \cdot 2H_2O$ are shown in Figures S3 and S4, respectively.

At AP, $V(NaBH_4 \cdot 2H_2O)$ is approximately 8.6% smaller than $V(NaBH_4 + 2H_2O)$, the sum of the volumes of 1 f. u. of $NaBH_4$ (α-phase) and 2 f. u. of liquid H_2O (water). This volume reduction

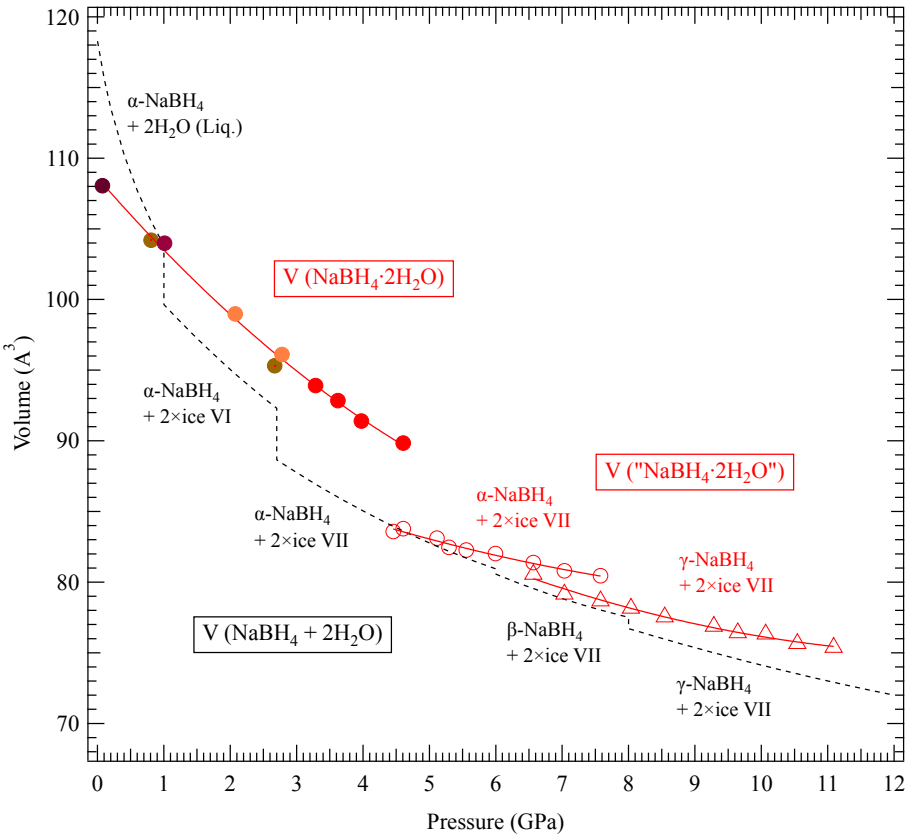

Figure 5. Pressure dependence of the volumes of the samples. Solid circles represent the volume of 1 f. u. of $NaBH_4 \cdot 2H_2O$ before dehydration. Different symbol colors indicate data obtained in different runs. Open symbols represent the combined volumes of 1 f. u. of $NaBH_4$ and two f. u. of ice VII after dehydration. The dashed line represents the sum of the volumes of 1 f. u. of $NaBH_4$ (measured in helium medium, Figure S2) and 2 f. u. of H_2O from the literature.[45, 46]

indicates that the formation of dihydrogen bonds leads to a more compact structure. However, as pressure increases, the volume of water decreases rapidly, and at around 1.0 GPa, V($NaBH_4 \cdot 2H_2O$) and V($NaBH_4 + 2H_2O$) become nearly equal, coinciding with the phase transition of H_2O from water to ice VI. Due to this transition, V($NaBH_4 + 2H_2O$) becomes about 4% smaller than V($NaBH_4 \cdot 2H_2O$). This reversal of the volume relationship suggests that, above 1 GPa, $NaBH_4 \cdot 2H_2O$ maintains a more open crystalline structure than ice VI, likely due to the presence of dihydrogen bonds. Furthermore, above 2.7 GPa, when ice VI transitions to ice VII, the volume difference between V($NaBH_4 \cdot 2H_2O$) and V($NaBH_4 + 2H_2O$) grows larger, and at approximately 4 GPa, V($NaBH_4 \cdot 2H_2O$) is about 9% larger than V($NaBH_4 + 2H_2O$).

The bulk modulus of $NaBH_4 \cdot 2H_2O$, calculated from the volume data up to 4.6 GPa, was B_0 = 21 GPa with V_0 = 108 $Å^3$, using the third-order Birch-Murnaghan equation of state.[48] For comparison, the bulk modulus of the AP phase of NH_3BH_3, another dihydrogen-bonded hydride, has been reported to range from 9.3 to 10 GPa.[4–6] This suggests that $NaBH_4 \cdot 2H_2O$ is stiffer and more resistant to compression than the AP phase of NH_3BH_3.

After the dehydration of $NaBH_4 \cdot 2H_2O$ at approximately 4.6 GPa, V("$NaBH_4 \cdot 2H_2O$") and V($NaBH_4 + 2H_2O$) are nearly equal, indicating that the effect of dihydrogen bonds is completely lost following dehydration, resulting in a simple combination of $NaBH_4$ (α-phase) and H_2O (ice VII). Subsequently, V("$NaBH_4 \cdot 2H_2O$") continues to decrease with increasing pressure, though at a slower rate than V($NaBH_4 + 2H_2O$). As α-$NaBH_4$ transitions to γ-$NaBH_4$, V("$NaBH_4 \cdot 2H_2O$") again approaches V($NaBH_4 + 2H_2O$), although the trend of a slower rate of decrease persists under further compression.

The volume change of V("$NaBH_4 \cdot 2H_2O$") is smaller than that of V($NaBH_4 + 2H_2O$), likely due to the poorer hydrostatic conditions under which the former was measured. In principle, when

samples are subjected to poor hydrostaticity, their volume appears larger than expected.[49, 50] Under conditions close to uniaxial compression, except for auxetic metamaterials, which have a negative Poisson's ratio, the sample experiences compressive stress along the direction parallel to the incident X-ray beam and tensile stress in the perpendicular direction. In XRD measurements using DAC, the transmitted scattered X-rays are measured in a geometry where the pressure axis is parallel to the X-ray incidence direction. As a result, the diffracted X-rays primarily capture information from the direction of tensile stress, leading to overestimated lattice parameters and volume measurements (see Figure S5(a), (b)). Hydrostaticity tends to decrease with increasing pressure but in this experiment it appears to improve temporarily during decomposition reactions and phase transitions. This trend is consistent with the pressure dependence of V($NaBH_4 \cdot 2H_2O$) and V("$NaBH_4 \cdot 2H_2O$") shown in Figure 5, as well as the volumes of $NaBH_4$ and ice VII presented in Figures S3 and S4, respectively.

In addition, the ruby balls used for pressure measurement are typically placed near the center of the sample chamber, where the measured pressure may be higher than the average pressure experienced by the entire sample (see Figure S5(c)).

Pressure dependence of bond distances and the number of the dihydrogen bonds in $NaBH_4 \cdot 2H_2O$

To investigate the pressure dependence of bond distances in the $NaBH_4 \cdot 2H_2O$, particularly the dihydrogen bond distances, DFT calculations were performed using the lattice parameters obtained from the Rietveld refinement of the XRD patterns.

The molecular arrangement around the BH_4^- ion in the crystal structure of $NaBH_4 \cdot 2H_2O$ at near AP (~0.08 GPa) and 4.0 GPa is shown in Figure 6, with crystallographic data provided in Table S2 and S3. The lattice parameters are generally consistent with previous data at 150 K, as reported by Filinchuk et al.[24], although the lattice parameters *a* and *b* are slightly smaller, and *c* is larger. When the distance between the hydrogen of the water molecule and that of the BH_4^- ion is represented as Hw–H, the criterion for dihydrogen bonds is defined as Hw–H < 2.4 Å, which is twice the van der Waals radius of hydrogen. The presence or absence of dihydrogen bonds may be

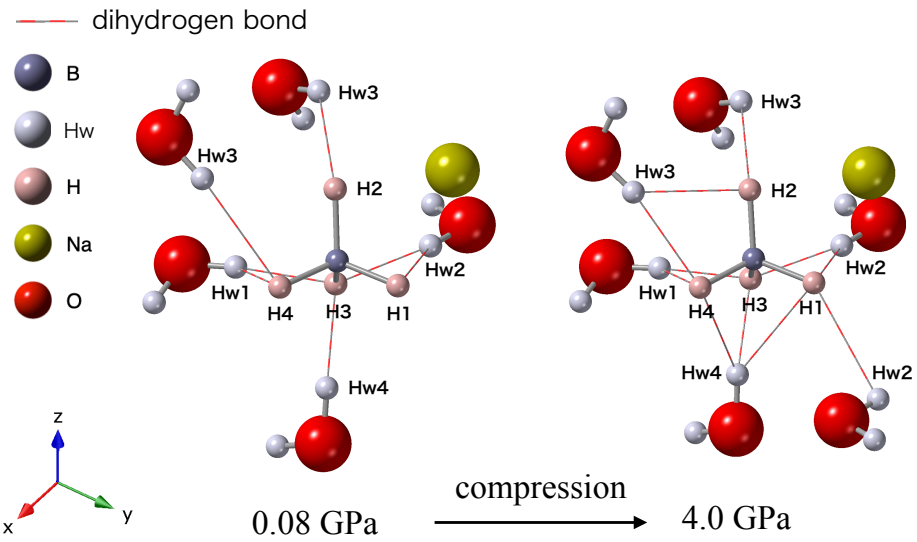

Figure 6. Molecular arrangement around the BH_4^- ion in the crystal structure of $NaBH_4 \cdot 2H_2O$ at near ambient pressure (~0.08 GPa) and 3.6 GPa. Yellow, blue, red, gray, and pink spheres represent sodium, boron, oxygen, water hydrogen (Hw), and BH_4^- hydrogen (H), respectively. Lines between Hw and H represent the dihydrogen bonds, where Hw–H distance is shorter than 2.4 Å. All of the Hw form dihydrogen bonds. The Hw that does not have the dihydrogen bond line in the figure forms a dihydrogen bond with the H atom of a BH_4^- that is different from the BH_4^- in the illustration.

evaluated with more in-depth examinations of other indicators, such as the perspective of molecular topology, in addition to the Hw–H distance. However, this is beyond the scope of the authors' expertise, therefore in this study, the Hw–H distance (< 2.4 Å) is simply used as an indicator of the presence of dihydrogen bonds.

At 0.08 GPa all water molecule hydrogens (Hw) form dihydrogen bonds with the hydrogens in the BH_4^- ions (H). There are seven types of dihydrogen bonds at this pressure, with Hw–H distances as shown in Table 1. In comparison, the dihydrogen bonds calculated from the atomic

Table 1. Comparison of dihydrogen bond length Hw–H in $NaBH_4 \cdot 2H_2O$ near ambient pressure. For the results obtained in this study, the distances exceeding 2.4 Å are shown in parentheses. Custelcean and Jackson did not provide detailed crystallographic data, and therefore the corresponding dihydrogen bond Hw–H was estimated from the length.

Hw–H	Dihydrogen bond length (Å)			
	This work 0.08 GPa, RT		Filinchuk et al.[24] 1 bar, 150 K	Custelcean and Jackson[23]
	with dispersion correction	without dispersion correction		
Hw1–H3	1.77	1.79	1.98	1.79
Hw1–H4	2.31	2.27	2.38	
Hw2–H1	2.40	(2.51)		
Hw2–H3	1.82	1.83	2.08	1.86
Hw3–H2	2.29	(2.41)		
Hw3–H4	2.29	2.30		
Hw4–H3	1.79	1.78	2.21	1.94

positions reported by Filinchuk et al.[24] at 1 bar and 150 K consist of four types with Hw–H distances. Custelcean and Jackson[23] reported three types of dihydrogen bonds for $NaBH_4 \cdot 2H_2O$ under ambient conditions, with distances of 1.79, 1.86, and 1.94 Å. In the case of our DFT calculation without dispersion correction, the number of dihydrogen bonds was reduced to five. Therefore, the difference in the number of dihydrogen bonds and the Hw–H distances may result from slight variations in the hydrogen atom positions due to DFT calculation conditions rather than differences in pressure and temperature. The symmetrized stress tensor of $NaBH_4 \cdot 2H_2O$ at 4.0 GPa obtained using DFT calculation with and without dispersion correction in this study was compared in Table S4.

Figure 7 illustrates the pressure dependence of several bond distances: (a) Hw–H distances between the hydrogens in the water molecules (Hw) and the hydrogens in the BH_4^- ions (H); (b) B–H bond distances between boron (B) and the four hydrogens in the BH_4^- ion (H); and (c) O–Hw distances between oxygen (O) and the hydrogens in the two water molecules (Hw).

As pressure increases, all Hw–H distances decrease, and the number of dihydrogen bonds rises. At approximately 4.5 GPa just before the dehydration of $NaBH_4 \cdot 2H_2O$, the number of dihydrogen bonds reaches twelve. Since there are four hydrogen atoms (Hw) in two water molecules, each Hw forms dihydrogen bonds with around three hydrogens in the BH_4^- ions.

Regarding the B–H distance in the BH_4^- ion and the O–Hw distance in the H_2O molecule, the former decreases by 0.5–0.8% under compression up to ~4.5 GPa, while the latter changed by less than 0.1%. This indicates that the BH_4^- ion undergoes greater shrinkage due to compression than the water molecule. Although the changes in O–Hw distances are minimal, there seems to be an expansion-shrinkage relationship within each H_2O molecule: O1–Hw1 expands while O1-Hw2 shrinks in the Hw1–O1–Hw2 molecule; similarly O2–Hw3 expands while O2-Hw4 shrinks in the

Hw3–O2–Hw4 molecule. However, since it is difficult to obtain bond lengths with an accuracy of less than 0.01 Å using DFT calculations, it is questionable whether this is a significant result.

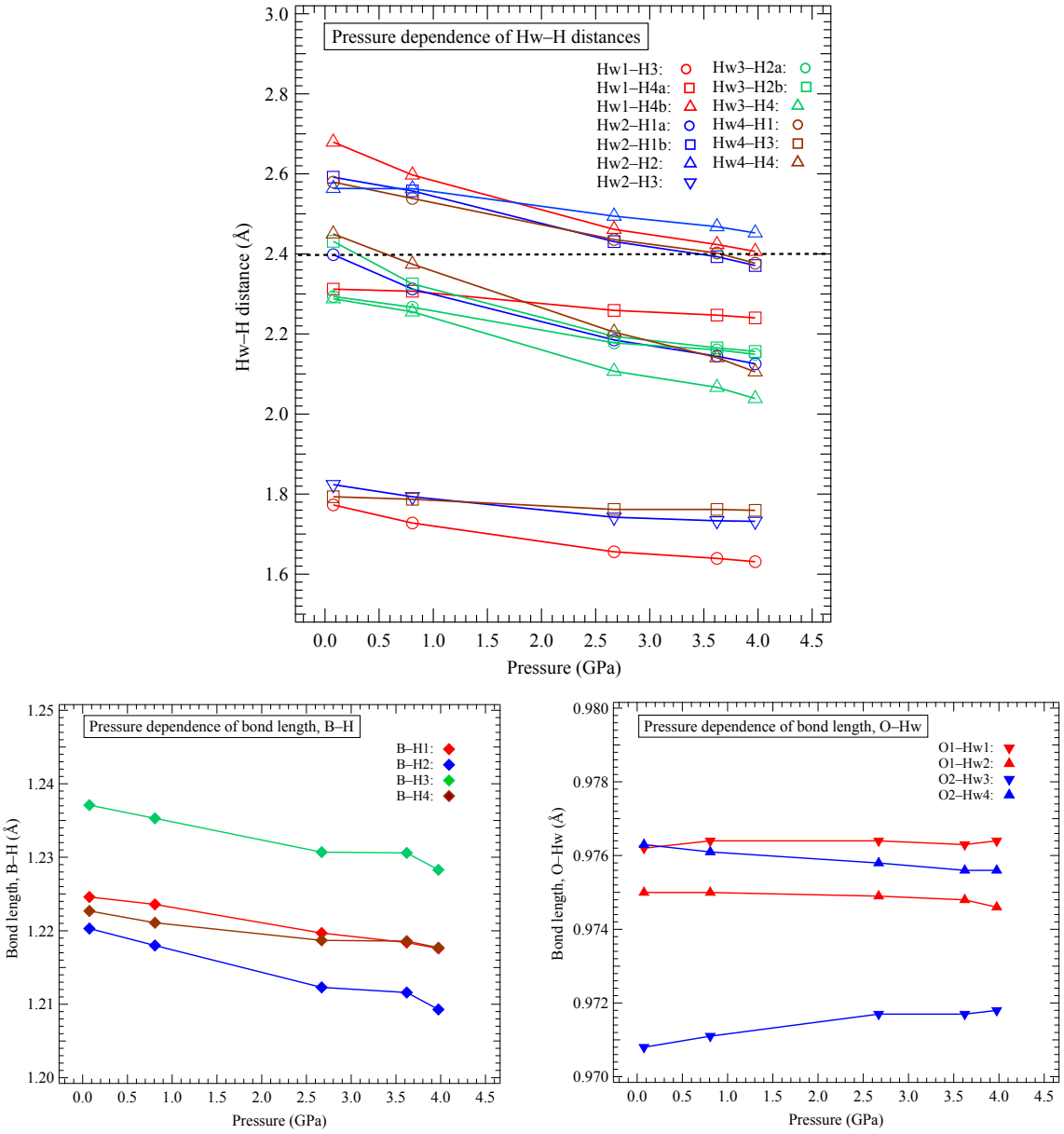

Figure 7. Pressure dependence of bond distances obtained using DFT calculation: (a) Hw–H distances between water molecule hydrogens (Hw) and BH_4^- hydrogens (H); (b) B–H bond distances between boron (B) and BH_4^- hydrogens (H); and (c) O–Hw distances between oxygen (O) and water molecule hydrogens (Hw).

In the DFT calculations, a comparison of the band structure at 0 GPa and 4.0 GPa showed no significant change except for an increase in the band gap from 6.3 eV to 6.8 eV (see Figure S6). No precursors of dehydration, such as molecular rearrangements and decomposition reactions, were observed in the electronic state.

CONCLUSIONS

The HP structural changes of the dihydrogen-bonded borohydride complex $NaBH_4 \cdot 2H_2O$ were studied up to ~11 GPa using XRD and Raman scattering spectroscopy. $NaBH_4 \cdot 2H_2O$ decomposed into the AP phase of $NaBH_4$ (α-$NaBH_4$) and ice VII at approximately 4.6 GPa. Upon reducing the pressure, $NaBH_4$ and ice VII reacted between 4.4 and 2.7 GPa, resulting in the recrystallization of $NaBH_4 \cdot 2H_2O$. This process, referred to as "decompression-induced recrystallization," demonstrates that the dihydrogen bonds in $NaBH_4 \cdot 2H_2O$ are robust and significant. DFT calculations were used to investigate the pressure dependence of the Hw–H distances in $NaBH_4 \cdot 2H_2O$, revealing seven distinct dihydrogen bonds at AP. As pressure increased, the Hw–H distances decreased, and the number of dihydrogen bonds rose to twelve at ~4.5 GPa just before dehydration. This suggests that each hydrogen atom in a water molecule forms dihydrogen bonds with approximately three hydrogens in BH_4^-. In addition, after dehydration, $NaBH_4$ underwent a reversible, pressure-induced transformation above 6.6 GPa, gradually transforming into the HP phase γ-$NaBH_4$.

In this study, it was found that cleavage and recombination of dihydrogen bonds can occur reversibly by tuning the pressure, which is an important clue for the synthesis of new dihydrogen-bonded compounds. For example, new hydride complexes can be expected to be synthesized using

other borohydrides and alanates in the presence of proton donor molecules. They may lead to the creation of new energy storage materials.

ASSOCIATED CONTENT

Supporting Information Available:

This information is available free of charge at the website: http://pubs.acs.org/

Supporting Information: Williamson-Hall plot for α-$NaBH_4$ and ice VII decomposed from $NaBH_4 \cdot 2H_2O$, and their crystallite sizes and strains estimated; the pressure dependence of the XRD pattern of $NaBH_4$ with helium pressure medium; the pressure dependence of the molar volume of $NaBH_4$ decomposed from $NaBH_4 \cdot 2H_2O$ and that of $NaBH_4$ measured with helium pressure medium; comparison of the dehydration of $NaBH_4 \cdot 2H_2O$ with those of hydrous compounds including hydrogen bond; the pressure dependence of the molar volume of ice VII decomposed from $NaBH_4 \cdot 2H_2O$ and that of ice; schematic illustrations of the influence of nonhydrostatic conditions on the lattice parameters of samples in HP XRD measurements using DAC; crystallographic information of $NaBH_4 \cdot 2H_2O$; symmetrized stress tensors calculated using DFT calculation with and without dispersion correction; Energy band calculated using DFT calculation; crystallographic parameters of $NaBH_4 \cdot 2H_2O$ (PDF)

AUTHOR INFORMATION

Corresponding Author

Satoshi Nakano – *National Institute for Materials Science (NIMS), 1-1 Namiki, Tsukuba, Ibaraki 305-0044, Japan*; https://orcid.org/0000-0002-7010-9867; E-mail: nakano.satoshi@nims.go.jp

Authors

Hiroshi Fujihisa – *National Metrology Institute of Japan (NMIJ), National Institute of Advanced Industrial Science and Technology (AIST), Tsukuba Central 5, 1-1-1 Higashi, Tsukuba, Ibaraki 305-8565, Japan*; https://orcid.org/0000-0001-9308-153X

Hiroshi Yamawaki – *National Metrology Institute of Japan (NMIJ), National Institute of Advanced Industrial Science and Technology (AIST), Tsukuba Central 5, 1-1-1 Higashi, Tsukuba, Ibaraki 305-8565, Japan*; https://orcid.org/0000-0002-0145-9935

Yuki Shibazaki – *Photon Factory (PF), Institute of Materials Structure Science (IMSS), High Energy Accelerator Research Organization (KEK), 1-1 Oho, Tsukuba, Ibaraki 305-0801, Japan;* https://orcid.org/0000-0002-0550-6719

Takumi Kikegawa – *Photon Factory (PF), Institute of Materials Structure Science (IMSS), High Energy Accelerator Research Organization (KEK), 1-1 Oho, Tsukuba, Ibaraki 305-0801, Japan;* https://orcid.org/0000-0001-8207-9987

Shin-ichi Orimo – *Advanced Institute for Materials Research (WPI-AIMR), Tohoku University, Katahira 2-1-1, Aoba-ku, Sendai, Miyagi 980-8577, Japan; Institute for Materials Research (IMR), Tohoku University, Katahira 2-1-1, Aoba-ku, Sendai, Miyagi 980-8577, Japan;* https://orcid.org/0000-0002-4216-0446

Author Contributions

S.N. designed the study, collected the experimental data, and mainly wrote the manuscript. H.F. and H.Y. conducted the DFT calculation, discussed the experimental and theoretical results and revised the manuscript. Y.S. and T.K. provided support for XRD measurements at the synchrotron facility. This work was conducted as one of the "Hydrogenomics" research projects supervised by

S.O. The manuscript was written through contributions of all authors. All authors have given approval to the final version of the manuscript.

Notes

The authors declare no competing financial interest.

ACKNOWLEDGMENT

The crystallographic data previously published was obtained from the AtomWork-Adv provided by the Materials Data Platform (MDPF) of the National Institute for Materials Science (NIMS), and this work was supported in part by Research Network and Facility Services Division in NIMS. The authors are very grateful to Mr. Y. Masuda, Mr. M. Iida, and Mr. T. Ikeda (NIMS) for their assistance with the machining process. We also thank Mr. K. Watanabe (Mitsubishi Electric System & Service Co., Ltd.) for supporting this work by maintaining the equipment in the synchrotron radiation X-ray beamline at KEK-PF, and Mr. K. Kainuma (Atago Giken Co., Ltd.) for his technical support for Raman scattering and ruby fluorescence measurements. The authors would like to appreciate Dr. T. Sumita (AIST) and Professor H. Kagi (Univ. Tokyo) for their useful suggestions about the EoS fitting and the dehydration of hydrous minerals, respectively. This work was partially supported by MEXT/JSPS KAKENHI (grant numbers JP23103706, JP18K05284 and JP21H00030). Synchrotron radiation X-ray diffraction experiments were performed at BL-18C and AE-NE1A in KEK-PF under the approval of proposal numbers 2011G584, 2013G684, and 2023G571.

REFERENCES

(1) Fukutani, K.; Yoshinobu, J.; Yamauchi, M.; Shima T.; Orimo, S. Hydrogenomics: Efficient and Selective Hydrogenation of Stable Molecules Utilizing Three Aspects of Hydrogen *Catalysis Lett*. **2022**, *152* (6), 1583–1597, DOI: 10.1007/s10562-021-03750-1

(2) Grabowski, S. J. In *Noncovalent Forces*; Scheiner, S. Ed.; Challenges and Advances in Computational Chemistry and Physics 19; Springer: Switzerland, 2015: Chapter 17.

(3) Staubitz, A.; Robertson, A. P. M.; Manners, I. Ammonia-Borane and Related Compounds as Dihydrogen Sources *Chem. Rev*. **2010**, *110* (7), 4079−4124, DOI: 10.1021/cr100088b

(4) Filinchuk, Y.; Nevidomskyy, A. H.; Chernyshov, D.; Dmitriev, V. High-pressure phase and transition phenomena in ammonia borane NH_3BH_3 from x-ray diffraction, Landau theory, and ab initio calculations *Phys. Rev. B* **2009**, *79* (21), 214111-1−11, DOI: 10.1103/PhysRevB.79.214111

(5) Kumar, R. S.; Ke, X.; Zhang, J.; Lin, Z.; Vogel, S. C.; Hartl, M.; Sinogeikin, S.; Daemen, L.; Cornelius, A. L.; Chen, C.; Zhao, Y. Pressure induced structural changes in the potential hydrogen storage compound ammonia borane: A combined X-ray, neutron and theoretical investigation *Chem. Phys. Lett*. **2010**, *495* (4–6), 203–207, DOI: 10.1016/j.cplett.2010.06.044

(6) Chen, J.; Couvy, H.; Liu, H.; Drozd, V.; Daemen, L. L.; Zhao, Y.; Kao, C.-C. In situ X-ray study of ammonia borane at high pressures *Int. J. Hydrogen Energy* **2010**, *35* (20), 11064–11070, https://doi.org/10.1016/j.ijhydene.2010.07.085

(7) Liang, Y.; Tse, J. S. First-Principles Study on the Mechanisms for H_2 Formation in Ammonia Borane at Ambient and High Pressure *J. Phys. Chem. C* **2012**, *116* (3), 2146–2152, DOI: 10.1021/jp206161m

(8) Nylén, J.; Eriksson, L.; Benson, D.; Häussermann, U. Characterization of a High Pressure, High Temperature Modification of Ammonia Borane (BH_3NH_3) *J. Chem. Phys.* **2013**, *139* (5), 054507-1−7, DOI: 10.1063/1.4817188

(9) Huang, Y.; Huang, X.; Zhao, Z.; Li, W.; Jiang, S.; Duan, D.; Bao, K.; Zhou, Q.; Liu, B.; Cui, T. Experimental verification of the high pressure crystal structures in NH_3BH_3 *J. Chem. Phys.* **2014**, *140* (24), 244507-1−9, DOI: 10.1063/1.4884819

(10) Nakano, S.; Sano-Furukawa, A.; Hattori, T.; Machida, S.; Komatsu, K.; Fujihisa, H.; Yamawaki, H.; Gotoh, Y.; Kikegawa, T. Observation of Dihydrogen Bonds in High-Pressure Phases of Ammonia Borane by X-ray and Neutron Diffraction Measurements *Inorg. Chem.* **2021**, *60* (5), 3065–3073, DOI: 10.1021/acs.inorgchem.0c03345

(11) Nakano, S.; Fujihisa, H.; Yamawaki, H.; Kikegawa, T. Influence of Pressure-Induced Formation of Dihydrogen Bonds on Lattice Parameters, Volume, and Vibrational Modes of Ammonia Borane *J. Chem. Phys.* **2022**, *157* (23), 234702-1–10, DOI: 10.1063/5.0128003

(12) Nakano, S.; Fujihisa, H.; Yamawaki, H.; Kikegawa, T. Phase Diagram Analysis of High-Pressure/High-Temperature Polymorphs of Ammonia Borane *Inorg. Chem.* **2024**, *63* (7), 3283−3291, DOI: 10.1021/acs.inorgchem.3c03615

(13) Yamawaki, H.; Fujihisa, H.; Gotoh, Y.; Nakano, S. Formation of $LiBH_4$ hydrate with dihydrogen bonding *J. Alloys Compd.* **2012**, *541*, 111–114, DOI: 10.1016/j.jallcom.2012.06.123

(14) Bakhmutov, V. I. Intermoleculer Dihydrogen-Bonded Complexes: From Groups 1A–4A to Xenon Dihydrogen-Bonded Complexes, Group 3A: Dihydrogen Bonds X–H···H–B, H–X···H–Al,

and X–H···H–Ga. *Dihydrogen Bonds – Principles, Experiments, and Applications*; John Wiley & Sons, Inc.: New Jersey, 2008; pp 128–136.

(15) Stockmayer, W. H.; Rice, D. W.; Stephenson, C. C. Thermodynamic Properties of Sodium Borohydride and Aqueous Borohydride Ion *J. Am. Chem. Soc.* **1955**, *77* (77), 1980–1983, DOI: 10.1021/ja01612a082

(16) Mikheeva V. I.; Breitsis, V. B. Temperature variation of solubility in the $NaBH_4$–H_2O system and solubility isotherms at 0°, 18°, 30°, and 50° for the $NaBH_4$–NaOH–H_2O system *Russ. J. Inorg. Chem.* **1960**, *5* (11), 1234–1238.

(17) Minkina, V. G.; Shabunya, S. I.; Kalinin, V. I.; Martynenko, V. V. Stability of aqueous-alkaline sodium borohydride formulations *Russ. J. Appl. Chem.* **2008**, *81* (3), 380–385, DOI: 10.1134/S1070427208030051

(18) Vilarinho-Franco, T.; Chiriac, R.; Tenu, R.; Counioux, J. J.; Delmas, J.; Capron, P.; Goutaudier, C. Polythermal diagrams of aqueous boundary ternary systems involving sodium borohydride hydrolysis for hydrogen generation *Fluid Phase Equilibria* **2018**, *460*, 189–197. DOI: 10.1016/j.fluid.2017.12.014

(19) Saldin, V. I.; Brovkina, O. V.; Ippolitov, E. G.; Popov, A. P. The MBF_4–MBH_4–H_2O systems (M = Na or K) at 0 °C *Russ. J. Inorg. Chem.* **1983**, *28* (2) 273–275.

(20) Arkhangelskii, I. V.; Tarasov, V. P.; Kravchenko, O. V.; Kirakosyan, G.; Tsvetkov, M. V.; Solovev, M. V.; Dobrovolskii, Yu. A.; Shihovzev, A. V. Thermoanalytical and NMR investigation of $NaBH_4 \cdot 2H_2O$ thermolysis process *J. Therm. Anal. Calorim.*, **2018**, *131*, 2833–2842, DOI: 10.1007/s10973-017-6821-3

(21) Arkhangel'sky, I. V.; Kravchenko, O. V.; Tsvetkov, M. V.; Dobrovol'sky, Yu. A.; Shikhovtsev, A. V.; Solovev, M. V.; Zaitsev, A. A. Synthesis of Sodium Borohydride Dihydrate and Specifi c Features of Its Thermolysis *Russ. J. Appl. Chem.* **2019**, *92* (6), 734–742, DOI: 10.1134/S1070427219060028

(22) Shikhovtsev, A. V.; Kravchenko, O. V.; Vinokurov, A. A.; Solov'ev, M. V.; Tsvetkov, M. V.; Dobrovol'skii, Yu. A. Saturation Vapor Pressure of Water over Sodium Borohydride Dihydrate *Russ. J. Appl. Chem.* **2023**, *96* (5), 562–565, DOI: 10.1134/S1070427223050075

(23) Custelcean, R.; Jackson, J. E. Dihydrogen Bonding: Structures, Energetics, and Dynamics *Chem. Rev.* **2001**, *101* (7), 1963−1980, DOI: 10.1021/cr000021b

(24) Filinchuk Y.; Hagemann, H. Structure and Properties of $NaBH_4 \cdot 2H_2O$ and $NaBH_4$ *Eur. J. Inorg. Chem.* **2008**, *2008* (20), 3127–3133. DOI: 10.1002/ejic.200800053

(25) Hamada, I.; Yamauchi, K.; Oguchi, T. Structure and intermolecular bonding in $NaBH_4 \cdot 2H_2O$: A density functional theory study *Phys. Rev. B* **2012**, *85* (21), 214119-1–4, DOI: 10.1103/PhysRevB.85.214119

(26) Takemura, K.; Sahu, P. C.; Kunii, Y.; Toma, Y. Versatile Gas-Loading System for Diamond-Anvil Cells *Rev. Sci. Instru.* **2001**, 72 (10), 3873−3876, DOI: 10.1063/1.1396667

(27) Seto, Y.; Hamane, D.; Nagai, T.; Fujino, K. Fate of Carbonates within Oceanic Plates Subducted to the Lower Mantle, and a Possible Mechanism of Diamond Formation *Phys. Chem. Minerals* **2008**, *35* (4), 223−229, DOI: 10.1007/s00269-008-0215-9

(28) Dassault Systèmes Americas Corp., BIOVIA materials studio reflex website. https://www.3ds.com/products/biovia/materials-studio/ (accessed 17 September 2024).

(29) Mao, H. K.; Bell, P. M.; Shaner, J. W.; Steinberg, D. J. Specific volume measurements of Cu, Mo, Pd, and Ag and calibration of the ruby R1 fluorescence pressure gauge from 0.06 to 1 Mbar *J. Appl. Phys.* **1978**, *49* (6), 3276–3283, DOI: 10.1063/1.325277

(30) Zha, C.-S.; Mao, H.-k.; Hemley, R. J. Elasticity of MgO and a primary pressure scale to 55 GPa *Proc. Natl. Acad. Sci.* **2000**, *97* (25) 13494–13499, DOI: 10.1073/pnas.240466697

(31) Clark, S. J.; Segall, M. D.; Pickard, C. J.; Hasnip, P. J.; Probert, M. I. J.; Refson, K.; Payne, M. C. First Principles Methods using CASTEP *Z. Kristallogr.* **2005**, *220* (5–6), 567−570, DOI: 10.1524/zkri.220.5.567.65075

(32) Perdew, J. P.; Burke, K.; Ernzerhof, M. Generalized gradient approximation made simple. *Phys. Rev. Lett.* **1996**, 77 (18), 3865–3868, DOI: 10.1103/PhysRevLett.77.3865.

(33) Vanderbilt, D. Soft Self-Consistent Pseudopotentials in a Generalized Eigenvalue Formalism *Phys. Rev. B* **1990**, *41* (11), 7892−7895, DOI: 10.1103/PhysRevB.41.7892

(34) Monkhorst, H. J.; Pack, J. D. Special Points for Brillouin-Zone Integrations *Phys. Rev. B* **1976**, *13* (12), 5188−5192, DOI: 10.1103/PhysRevB.13.5188

(35) Tkatchenko, A.; Scheffler, M. Accurate Molecular Van Der Waals Interactions from Ground-State Electron Density and Free-Atom Reference Data *Phys. Rev. Lett.* **2009**, *102* (7), 073005, DOI:10.1103/PhysRevLett.102.073005

(36) S. C. Abrahams; J. Kalnajs, The Lattice Constants of the Alkali Borohydrides and the Low-Temperature Phase of Sodium Borohydride *J. Chem. Phys.* **1954**, *22* (3), 434–436, DOI: 10.1063/1.1740085

(37) Kamb, B.; Davis, B. L. Ice VII, the densest form of ice *Proc. Natl. Acad. Sci.* **1964**, *52* (6) 1433–1439, DOI: 10.1073/pnas.52.6.1433

(38) Hansen, T. C. The everlasting hunt for new ice phases *Nature Commun,* **2021**, *12*, 3161, DOI: 10.1038/s41467-021-23403-6

(39) Scherrer, P. Bestimmung der Größe und der inneren Struktur von Kolloidteilchen mittels Röntgenstrahlen *Nachrichten von der Gesellschaft der Wissenschaften zu Göttingen, Mathematisch-Physikalische Klasse* **1918**, *1918*, 98–100, http://eudml.org/doc/59018

(40) Williamson, G. K.; Hall, W. H. X-ray line broadening from filed aluminium and wolfram *Acta Metall.* **1953**, *1*, 22–31, DOI: 10.1016/0001-6160(53)90006-6

(41) Filinchuk, Y.; Talyzin, A. V.; Chernyshov, D.; Dmitriev, V. High-pressure phase of $NaBH_4$: Crystal structure from synchrotron powder diffraction data *Phys. Rev. B* **2007**, *76* (9), 092104-1–4, DOI: 10.1103/PhysRevB.76.092104

(42) Kumar R. S.; Cornelius, A. L. Structural transitions in $NaBH_4$ under pressure *Appl. Phys. Lett.* **2005**, *87* (26), 261916-1–3, DOI: 10.1063/1.2158505

(43) Klotz, S.; Chervin, J.-C.; Munsch, P.; Marchand, G. L. Hydrostatic limits of 11 pressure transmitting media *J. Phys. D: Appl. Phys.* **2009**, *42* (7), 075413-1–7, DOI:10.1088/0022-3727/42/7/075413

(44) Marizy, A.; Geneste, G.; Garbarino. G.; Loubeyre, P. High pressure polymorphism of $LiBH_4$ and of $NaBH_4$ *RSC Adv*. **2021**, *11* (41), 25274–25283, DOI: 10.1039/d1ra00816a

(45) Pinceaux, J.-P.; Maury, J.-P.; Besson, J.-M. Solidification of helium, at room temperature under high pressure *J. Physique Lett*. **1979**, *40* (13), 307–308, DOI: 10.1051/jphyslet:019790040013030700

(46) Wagner W.; Pruß, A. The IAPWS Formulation 1995 for the Thermodynamic Properties of Ordinary Water Substance for General and Scientific Use *J. Phys. Chem. Ref. Data* **2002**, *31* (2), 387–535, DOI: 10.1063/1.1461829

(47) Bezacier, L.; Journaux, B.; Perrillat, J.-P.; Cardon, H.; Hanfland, M.; Daniel, I. Equations of state of ice VI and ice VII at high pressure and high temperature *J. Chem. Phys*. **2014**, *141* (10), 104505-1–6, DOI: 10.1063/1.4894421

(48) Katsura, T.; Tange, Y. A Simple Derivation of the Birch–Murnaghan Equations of State (EOSs) and Comparison with EOSs Derived from Other Definitions of Finite Strain *Minerals* **2019**, *9*, 745-1–19, DOI: 10.3390/min9120745

(49) Singh, A. K. X-ray diffraction from solids under nonhydrostatic compression—some recent studies *J. Phys. Chem. Solids* **2004**, *65* (8–9), 1589–1596, DOI: 10.1016/j.jpcs.2003.11.044

(50) Dubrovinsky, L.; Dubrovinskaia, N. Angle-dispersive diffraction under non-hydrostatic stress in diamond anvil cells *J. Alloys Compd.* **2004**, *375* (1–2), 86-92, DOI: 10.1016/j.jallcom.2003.12.007

SYNOPSIS

High-pressure structural changes of dihydrogen-bonded borohydride complex $NaBH_4 \cdot 2H_2O$ were studied up to ~11 GPa using XRD and Raman scattering spectroscopy to investigate the influence of dihydrogen bonds. At ~4.6 GPa, $NaBH_4 \cdot 2H_2O$ underwent dehydration and decomposed into α-$NaBH_4$ and ice VII. As pressure decreased, the decomposed α-$NaBH_4$ and ice VII reacted, resulting in the recrystallization of $NaBH_4 \cdot 2H_2O$. The reversible recrystallization suggests that dihydrogen bonds are as strong as conventional hydrogen bonds.

TOC/abstract graphics

For Table of Contents Only